Article

Journal of
Nanoscience and Nanotechnology
Vol. 17, 7264–7269, 2017
www.aspbs.com/jnn

Effects of SOG Passivation Layers Annealed in Various Ambient Conditions on the Stability of Amorphous InGaZnO Thin Film Transistors

Jin-Kuk Kim[1], Jinsung Choi[2], Byung Seong Bae[1], and Eui-Jung Yun[3,*]

[1] Department of Display Engineering, Hoseo University, Asan, Chungnam 31499, Korea
[2] Department of NanoBio Tronics, Hoseo University, Asan, Chungnam 31499, Korea
[3] Department of ICT Automotive Engineering, Hoseo University, Dangjin, Chungnam 31702, Korea

This study reports the effects of new siloxane-based spin-on-glass (SOG) passivation layers (PLs) annealed in various ambient conditions on the reliability of sputter-deposited amorphous-InGaZnO thin-film transistors (a-IGZO TFTs). The a-IGZO TFTs passivated by SOG annealed in O_2, N_2, and N_2O in a vacuum chamber showed better stability against positive bias stress (PBS) and negative bias stress (NBS) than those annealed in air. The a-IGZO TFTs made with the N_2-annealed SOG PLs showed the best mobility of greater than 10 cm^2/Vs as well as the best stability against NBS and PBS with a threshold voltage shift window of 1.1 V among all the TFTs prepared in this study. This was attributed to the reduction in the number of O-related acceptors and H-related donors in IGZO under PBS and NBS, respectively, as confirmed by secondary ion mass spectroscopy analysis. The experimental results suggest that this new methyl-siloxane-based SOG has good potential for use as an effective passivation material.

Keywords: InGaZnO Thin-Film Transistor, SOG, Passivation, Stability.

1. INTRODUCTION

To date, for the realization of high-performance metal oxide semiconductor thin-film transistors (TFTs) with a large field-effect mobility and on-off drain current ratio, amorphous indium-gallium-zinc oxide (a-IGZO) has been the most widely used channel material because of its superior physical properties compared with amorphous or polycrystalline silicon.[1–8] However, the instability of a-IGZO TFTs under the application of a constant gate bias stress has become an important issue in unpassivated TFTs with a bottom gate structure.[9–15] It has been reported.[16–18] that the reliability of a-IGZO TFTs is impaired by the ambient effects associated with the adsorption–desorption of oxygen and/or water molecules from the ambient atmosphere onto the exposed back-channel surface. Therefore, passivation layers have usually been required to enhance the stability of a-IGZO TFTs.

Recently, a variety of inorganic passivation layers, including SiO_x,[19,20] Al_2O_3,[19,21] Y_2O_3,[19] TiO_2,[19] MgO,[22] SiN_x,[16] AlO_x,[23] have been exploited. However, these inorganic passivation layers are generally deposited using complicated and high-cost vacuum processes which have negative effects on the performance of the TFTs owing to the plasma damage that creates trap states at the channel-gate insulator interface.[18] On the other hand, several organic passivation layers such as photoacryl,[24] paraffin wax,[25] and CYTOP[26] have also been suggested because they are much easier to deposit through a simple solution process or sol–gel method than their inorganic counterparts. Furthermore, photosensitive organic–inorganic hybrid passivation layers based on polysilsesquioxane[17,18] have been proposed for use in a-IGZO TFTs. However, organic passivation layers commonly degrade the transfer characteristics and reliability of a-IGZO TFTs. Hence, various organic passivation layers will need to be explored to improve the stability of a-IGZO TFTs. In this study, we examined the effects of a new methyl-siloxane-based organic passivation layer subjected to heat treatment in different ambient conditions on the device stability of a-IGZO TFTs against constant gate bias stresses.

*Author to whom correspondence should be addressed.

 1533-4880/2017/17/7264/006 doi:10.1166/jnn.2017.14747

2. EXPERIMENTAL DETAILS

The a-IGZO TFTs with the SOG passivation film were simply fabricated on a SiO_2 oxide layer thermally-grown onto a heavily-doped *p*-type Si substrate. Hence, the Si substrate and 300-nm-thick SiO_2 layer were used as the gate electrode and gate insulator, respectively. A 50-nm-thick a-IGZO channel layer was deposited at 200 °C using a sputter target with an In:Ga:Zn atomic ratio of 1:1:1 under the following conditions: an RF power of 50 W, working pressure of 5 mtorr and O_2 ratio of 25%. A shadow mask was used to pattern the a-IGZO channel layer. The channel layer was post-annealed at 400 °C for 1 hour in air after deposition. Subsequently, the methylsiloxane-based SOG passivation layer (PL), which contains CH_3 or C_2H as an organic dopant was deposited using a sol–gel method after the hexamethyldisilazane film was spin-coated to improve the adhesion between the SOG and channel layers. The SOG solution, which consisted of Cospeen®-1225G obtained from NEPES Corporation, was filtered through a 0.2 μm polytetrafluoroethylene filter and spin-coated at 3000 rpm for 30 s. Then, the spin-coated SOG was converted to SiO_x by thermal annealing at a fixed temperature of 200 °C for 1 hr in various ambient conditions viz. air, O_2, N_2, and N_2O to evaporate the solvent. Here, the heat-treatments in air were conducted in an air furnace while those conducted in O_2, N_2, and N_2O were performed inside a vacuum chamber with a pressure of 20 mtorr. The chemical structure of the siloxane-based SOG PL[27] is shown in Figure 1(a). The SOG PL was patterned by a photolithography process using the following dry etching conditions: an RF power of 196 W, working pressure of 100 mtorr, and mixed gas ratio of CF_4:O_2 = 60:20. Finally, the 150-nm-thick Al source–drain electrodes were deposited by DC magnetron sputtering and patterned using a shadow mask. The annealing of all of the developed TFTs was performed at 150 °C for 1 hour in air after they had been placed in a built-in heating element to form an ohmic contact between the channel and source–drain electrodes. Figure 1 shows a schematic cross-sectional view and photographic top view of the typical a-IGZO based TFTs with siloxane-based SOG PL developed in this study, confirming that the TFTs have a bottom gate and top contact structure. The channel width (W) and channel length (L) were the same, 1000 μm.

To investigate the changes in the depth profiles of O, C, and H in the a-IGZO TFT structures, secondary ion mass spectroscopy (SIMS) analyses were carried out using a Cs^+ gun under the following conditions: an impact energy of 14.5 keV, current of 10 nA, and raster size of 130 μm. The material composition of the siloxane-based SOG PL estimated from the SIMS results was C 50.5%, Si 44.9%, H 3.9%, and O 0.7%. A negative-bias-stress (NBS) and positive-bias-stress (PBS) were applied at room temperature (RT) in air using fixed gate-to-source voltages (V_{GS}) of −20 and 20 V, respectively. During NBS and PBS, the drain and source electrodes were grounded and a maximum stress time of 3.6×10^3 s was used. The gate-bias stress and device characteristics of the a-IGZO-based TFTs were measured in a darkened probe box by using two Keithley 2400 source meters as the DC voltage source and a Keithley 6485 picoammeter for the current measurements.

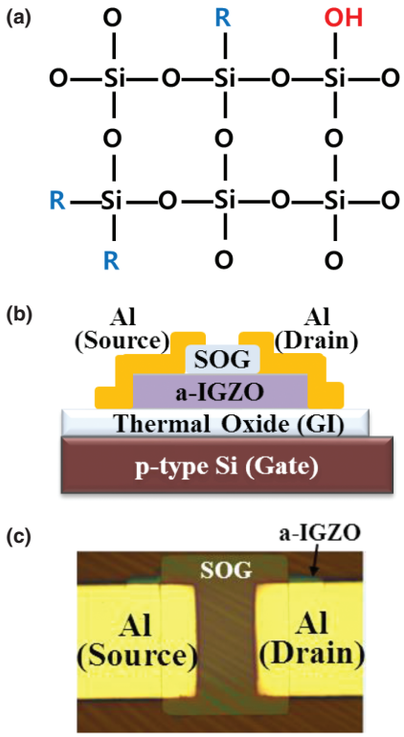

Figure 1. (a) Chemical structure of siloxane-based SOG passivation layer (R = CH_3 or C_2H).[27] (b) Schematic cross-sectional view and (c) photographic top view of the a-IGZO TFTs with a siloxane-based SOG passivation layer treated at 200 °C for 1 hr in various ambient conditions.

3. RESULTS AND DISCUSSION

Figures 2 and 3 show the evolutions of the drain-to-source current versus V_{GS} (I_{DS}–V_{GS}) transfer curves as a function of the stress time (τ_{st}) for the passivated a-IGZO TFTs with SOG annealed in four different ambient atmospheres, viz. air, O_2, N_2, and N_2O under PBS and NBS, respectively. All of the measurements were performed with a fixed drain-to-source voltage (V_{DS}) of 10 V, which is in the saturation region. The slopes of the sub-threshold swing (SS) were obtained from the inverse slopes of the transfer curves in Figures 2 and 3. The saturation field-effect mobility μ_{eff} was also estimated using Eq. (1):

$$\mu_{eff} = \left(\frac{\partial\sqrt{I_{DS}}}{\partial V_{GS}}\right)^2 \frac{2L}{W}\frac{1}{C_{ox}} \quad (1)$$

where C_{ox} is the capacitance per unit area of the SiO_2 gate insulator, which was ~11.8 nF/cm^2 as measured in a

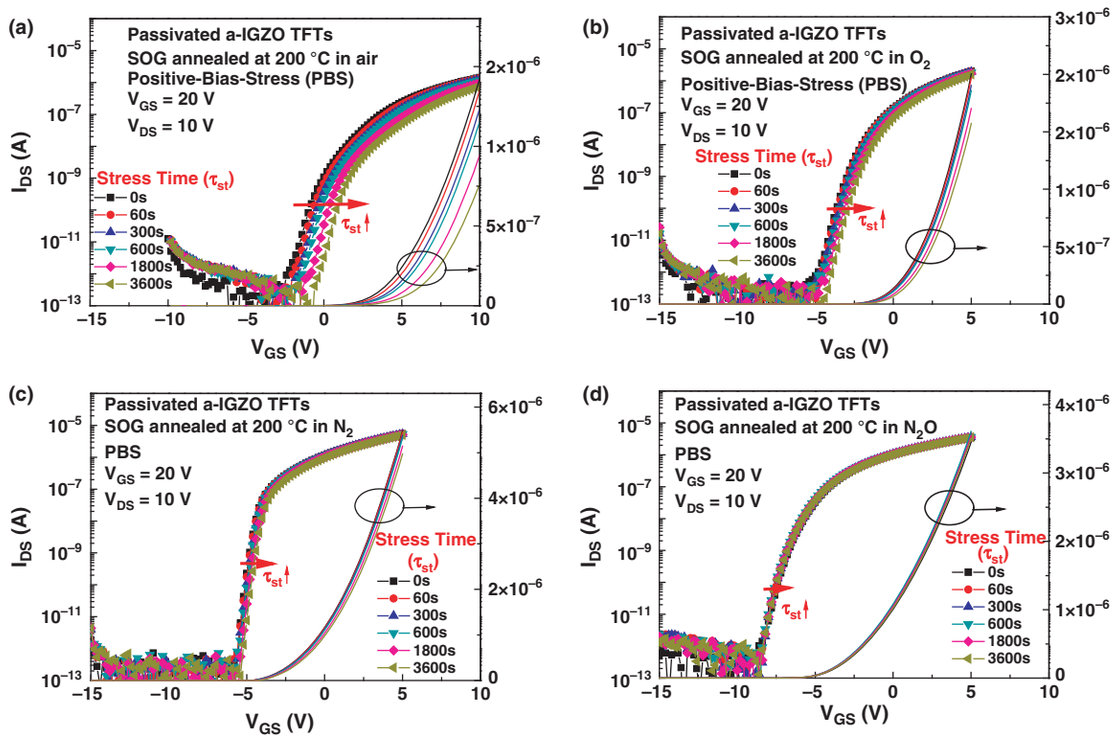

Figure 2. Evolutions of the I_{DS}–V_{GS} transfer curves as a function of the stress time (τ_{st}) for the passivated a-IGZO TFTs with SOG annealed in four different ambients, viz. (a) air, (b) O_2, (c) N_2, and (d) N_2O under PBS with a V_{GS} of 20 V.

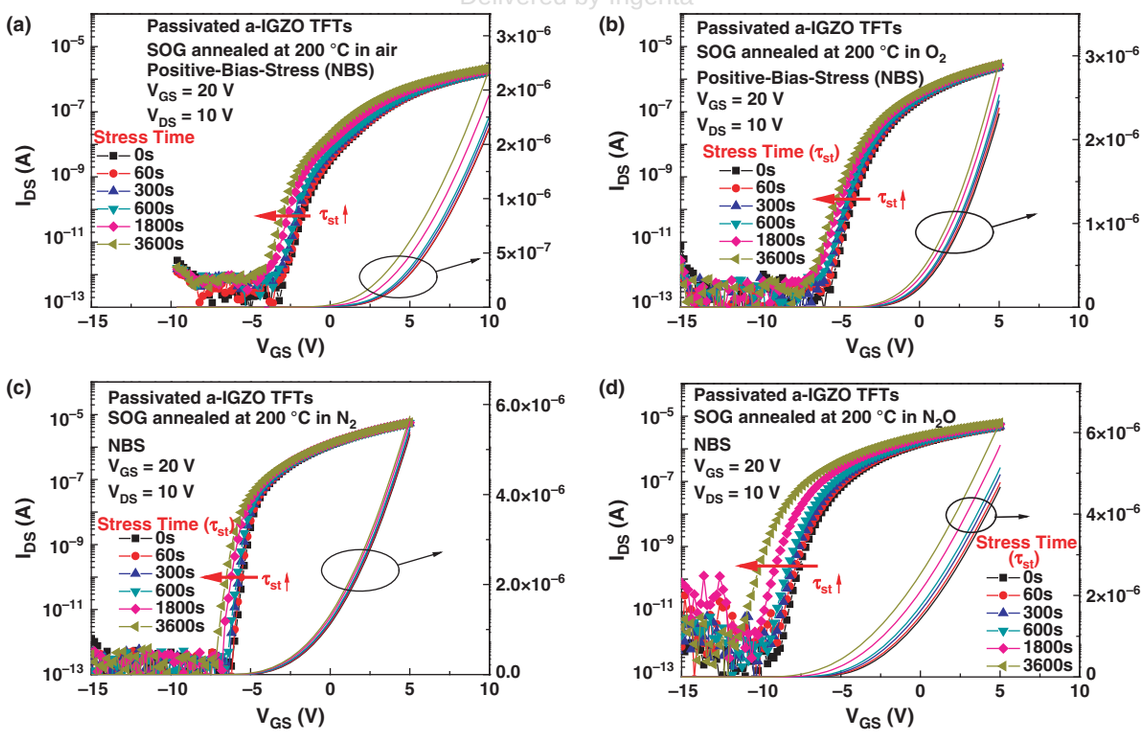

Figure 3. Evolutions of the I_{DS}–V_{GS} transfer curves as a function of the stress time (τ_{st}) for the passivated a-IGZO TFTs with SOG annealed in four different ambients, viz. (a) air, (b) O_2, (c) N_2, and (d) N_2O under NBS with a V_{GS} of −20 V.

Table I. Summary of the important device parameters at two stress times of 0 and 3600 s for the a-IGZO TFTs with SOG PLs under PBS and NBS, which were obtained from the results in Figures 2 and 3 using Eq. (1).

Anneal ambient type of SOG/stress	Stress time (s)	V_{th} (V)	μ_{eff} (cm^2/Vs)	SS (V/dec)	On/off ratio
Air/PBS	0	0.99	3.12	0.89	5.50×10^6
	3600	3.10	2.93	0.80	2.94×10^6
O_2/PBS	0	−2.59	9.28	0.67	6.73×10^7
	3600	−1.88	9.04	0.69	5.93×10^7
N_2/PBS	0	−4.95	10.69	0.29	3.38×10^7
	3600	−4.53	10.52	0.3	3.07×10^7
N_2O/PBS	0	−6.29	4.91	0.68	2.49×10^7
	3600	−6.18	5.03	0.68	2.6×10^7
Air/NBS	0	0.88	3.91	0.98	4.62×10^6
	3600	−0.92	3.56	0.77	6.13×10^6
O_2/NBS	0	−2.99	8.8	0.66	2.24×10^7
	3600	−3.99	8.5	0.74	2.57×10^7
N_2/NBS	0	−5.32	9.93	0.29	3.29×10^7
	3600	−6.02	9.52	0.34	3.54×10^7
N_2O/NBS	0	−6.2	6.75	0.66	1.53×10^7
	3600	−8.73	6.21	0.63	2.05×10^7

metal-insulator-metal configuration. Table I also summarizes the important device parameters at two τ_{st} values of 0 and 3600 s for the passivated samples under constant gate bias stresses, which were obtained from the results shown in Figures 2 and 3 using Eq. (1). As shown in Figures 2 and 3, and Table I, the following changes are observed:

(1) In the case of PBS, small positive V_{th} shifts ($\Delta V_{th\text{-}PBS} = V_{th\text{-}PBS}$ (3600 s) $-$ $V_{th\text{-}PBS}$ (0 s)) of 0.71, 0.42, and 0.11 V were observed without any significant changes in the SS for the TFTs with SOG annealed in a vacuum chamber in O_2, N_2, and N_2O ambients, respectively, while the TFTs with an air-annealed SOG exhibited a large $\Delta V_{th\text{-}PBS}$ of 2.11 V accompanying the change in SS.

(2) For NBS, low negative V_{th} shifts ($\Delta V_{th\text{-}NBS} = V_{th\text{-}NBS}$ (0 s) $-$ $V_{th\text{-}NBS}$ (3600 s)) of 1 and 0.7 V without any changes in the SS were observed for the TFTs with SOG PLs annealed in O_2 and N_2 ambients, respectively, whereas a large $\Delta V_{th\text{-}NBS}$ of 1.8 V was observed with a large SS change of 0.21 V/decade for the samples with an air-annealed SOG.

Here, $\Delta V_{th\text{-}PBS}$ represents the positive shift of V_{th} under PBS and $\Delta V_{th\text{-}NBS}$ denotes the negative shift of V_{th} under NBS. The above two results indicate that the stabilities against PBS and NBS for the TFTs with SOG annealed in ambient types of O_2 and N_2 are better than those for the samples with the air-annealed SOG. It should be emphasized that the best mobility of greater than 10 cm^2/Vs and the best stability against PBS and NBS were observed for the TFTs with the N_2-annealed SOG PLs, while the worst stability and the worst device parameters were observed for the TFTs with the air-annealed SOG among all the samples prepared in this study. However, no significant changes in the field-effect mobility or on/off ratio of I_{DS} were observed for either type of bias stress. It has been reported[24] that this parallel shift in V_{th} without any changes in the SS under PBS or NBS is due to simple charge trapping in the gate insulator and/or at the channel-insulator interface rather than the creation of defects within the channel materials. This suggests that the charge trapping model can by itself explain the PBS and NBS behaviors of the TFTs with SOG PLs annealed in O_2 and N_2 in this study. On the other hand, the PBS and NBS behaviors of the TFTs with air-annealed SOG PLs accompanying the change in the SS can be ascribed to the creation of some defects within the IGZO channel materials due to the introduction of elements from the SOG into the IGZO layer during the air-heat treatment. Hence, it is noteworthy that the better stabilities against PBS and NBS of the samples annealed in ambient types of O_2 and N_2 compared to those with an air-annealed SOG are mainly due to the reduction in the number of trapped charges in the SiO_2 gate insulator and/or at the a-IGZO channel-SiO_2 insulator interface. It is also likely that for the samples with an air-annealed SOG, in the case of NBS, the insertion of some elements from the SOG into the a-IGZO layer can induce deep level and donor-like trap states within the energy band gap of the a-IGZO channel layer, resulting in an increase in the SS and negative shift in V_{th} without any significant changes in the field-effect mobility.

To explore the plausible mechanism behind the changes in reliability of the a-IGZO TFTs with the annealed SOG PLs in the two ambient types of air and N_2, the changes in the SIMS depth profiles of oxygen (O), carbon (C), hydrogen (H), zinc (Zn), and silicon (Si) in the SOG/IGZO/SiO_2/Si TFT structures were monitored. We selected these two cases air and N_2 because they revealed, respectively, the worst and best stabilities against PBS and NBS. The SIMS depth profiles shown in Figure 4 exhibit the percentage variations in the O, C, and H concentrations in the TFT structures after heat treatment at 200 °C in air and N_2 ambients. The concentration changes are normalized with respect to the initial concentrations in the TFT structure with the air-annealed SOG PLs using Eq. (2):

$$\Delta I(\%) = \frac{I_{N2} - I_{air}}{I_{air}} \times 100 \qquad (2)$$

where I_{N2} and I_{air} are the element concentrations in the TFT structures with the N_2- and air-annealed SOG PLs, respectively. In Eq. (2), a negative (positive) value of ΔI means a decrease (increase) in the concentrations of O, C, and H in the TFT structure with N_2-annealed SOG PLs compared to the initial concentration in the TFT structure with air-annealed SOG PLs. There were no noted changes of C concentration in the a-IGZO, as shown in Figure 4(b). However, Figures 4(a) and (c), respectively, show the negative changes in the H and C concentrations indicating that the dominant amounts of H and O are decreased in the IGZO channel layers for the samples with N_2-annealed SOG PLs compared to those with air-annealed SOG PLs. It is well-known that H can act as shallow-donor defects while O becomes acceptor-like

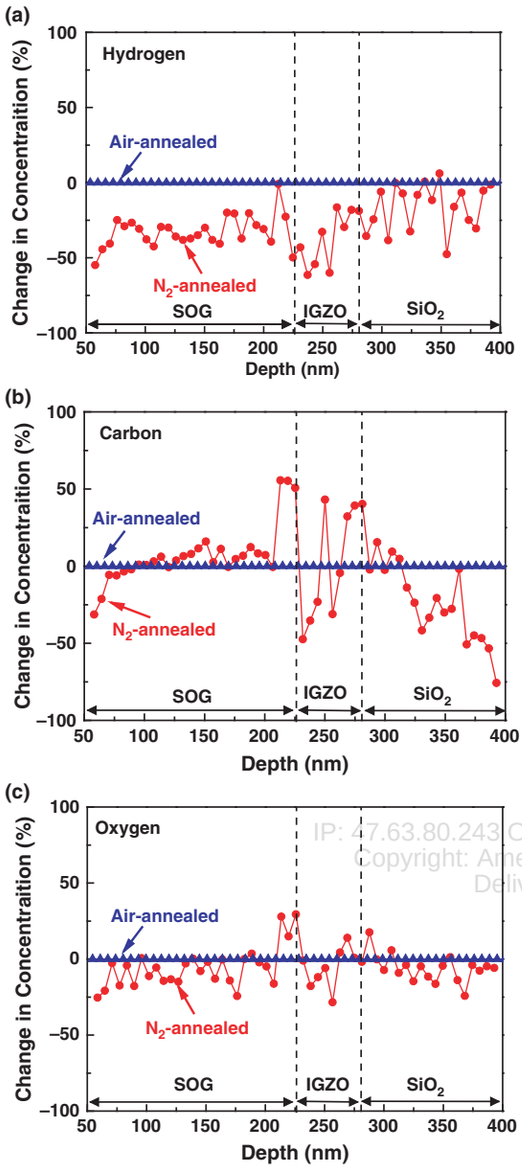

Figure 4. Percentage variations in (a) hydrogen (H), (b) carbon (C), and (c) oxygen (O) concentrations in the SOG/IGZO/SiO_2/Si TFT structures after the heat treatment at 200 °C in air and N_2 ambients were performed, which were obtained from the SIMS depth profiles.

defects in ZnO[28] and IGZO.[17,29] Therefore, as shown in Figure 4(a), the reduced H concentration apparently causes a reduction in the H-related donor defects, giving rise to a decrease in the electron concentration in the IGZO films, which in turn results in the enhancement of the stability against NBS in the case of the samples with an N_2 annealed SOG. Figure 4(c) also shows a decrease in the O concentration in the IGZO films for the samples with an N_2-annealed SOG compared to those with an air-annealed SOG, indicating that a notable amount of O diffused out from the IGZO films during the heat treatment in N_2. This causes a decrease in the hole concentration in the IGZO films as a result of the reduction in the number of O_i acceptor defects. As a result, from Figures 4(a) and (c), we can predict that the PBS stability is improved by the decrease in the number of O_i acceptor defects in the IGZO layer and the NBS instability is alleviated by the decrease in the number of H-related donor defects for the samples with an N_2-annealed SOG.

On the contrary, it can also be hypothesized that the H and O concentrations in the a-IGZO layer for the samples with the air-annealed SOG are higher than those for the samples with the N_2-annealed SOG. Therefore, we can conclude that for the samples with the air-annealed SOG the PBS and NBS instabilities originate from the insertion of O acceptor-like and H donor-like defects from the SOG into the IGZO layer, respectively, as compared to the samples with the N_2-annealed SOG. These results confirm the above hypothesis that for the samples with the air-annealed SOG under NBS, the insertion of some elements from the SOG into the a-IGZO layer can induce donor-like trap states within the energy band gap of the a-IGZO channel layer, which results in an increase in the SS and a negative shift in V_{th}.

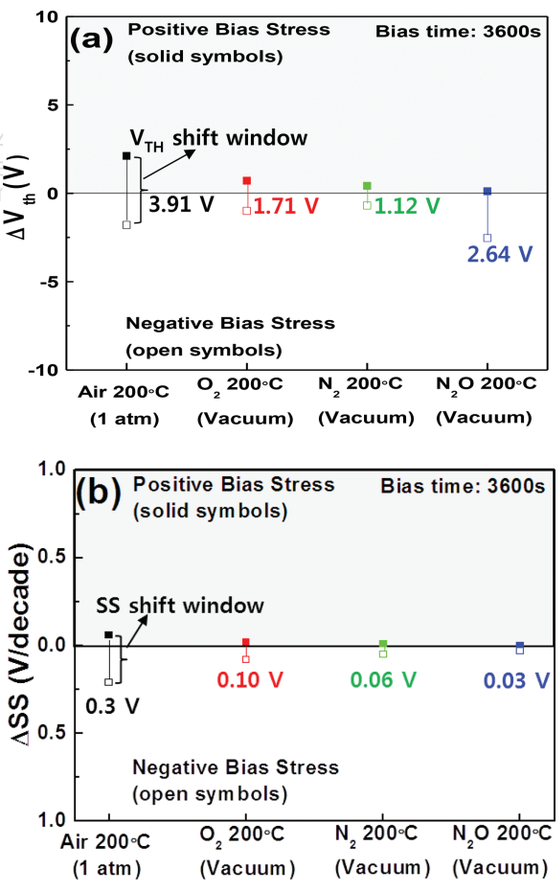

Figure 5. (a) V_{th} shift window ($V_{th\text{-}sw} = |\Delta V_{th\text{-}PBS}| + |\Delta V_{th\text{-}NBS}|$) and (b) SS shift window ($SS_{sw} = \Delta SS_{PBS} + \Delta SS_{NBS}$) under PBS and NBS for the a-IGZO TFTs with various SOGs annealed in different ambients viz. air, O_2, N_2, and N_2O. The measured data up to 3600 s were used in all cases.

To visualize more clearly the stabilities against PBS and NBS for all of the a-IGZO TFTs prepared in this study, the changes in V_{th} and SS under PBS and NBS were replotted using the data listed in Table I and the results are shown in Figure 5. For the N_2-annealed samples under PBS and NBS, the V_{th} shift window ($V_{th\text{-}sw}$) as well as the SS shift window (SS_{sw}) were the narrowest among all of the samples. Here, $V_{th\text{-}sw}$ is defined as the sum of the magnitude of the positive V_{th} shift under PBS ($\Delta V_{th\text{-}PBS}$) and the negative V_{th} shift under NBS ($\Delta V_{th\text{-}NBS}$) ($V_{th\text{-}sw} = |\Delta V_{th\text{-}PBS}| + |\Delta V_{th\text{-}NBS}|$), and SS_{sw} represents the summation of the SS shift under PBS (ΔSS_{PBS}) and the SS shift under NBS (ΔSS_{NBS}). As confirmed in Figure 5, among all of the samples prepared in this study, the IGZO TFTs with N_2-annealed SOG PLs exhibited the best stability against PBS and NBS with $V_{th\text{-}sw} = 1.12$ V and $SS_{sw} = 0.06$ V/dec. Based on the results shown in Figure 4 and Table I, in our N_2-annealed IGZO TFTs, the PBS instability is reduced mainly by the decrease of the hole density in the IGZO layer because of the removal of the O acceptor-like defects from IGZO after annealing the SOG in N_2, but the NBS instability is decreased by the decrease of the electron density in the IGZO layer due to the ejection of the H donor-like defects from IGZO after the annealing of the SOG in N_2.

4. CONCLUSION

We investigated the effects of a new methyl-siloxane-based organic passivation layer subjected to heat treatment in different ambient conditions on the device stability characteristics of the passivated a-IGZO TFTs against constant gate bias stresses. It was observed that the stabilities against PBS and NBS for the TFTs with SOG PLs annealed in O_2 and N_2 ambients were better than those for the samples with the air-annealed SOG PLs. The results also revealed that the best mobility of greater than 10 cm^2/Vs and the best stability against PBS and NBS with a V_{th} shift window of 1.12 V and SS shift window 0.06 V/dec. were observed for the TFTs with the N_2-annealed SOG PLs, while the worst stability and the worst device parameters were observed for the TFTs with the air-annealed SOG, among all of the samples prepared in this study. The superior stability of the N_2-annealed IGZO TFTs was attributed to the fact that the PBS instability was alleviated by the decrease of the hole density in the IGZO layer, due to the exclusion of O acceptor-like defects from IGZO after SOG annealing in N_2 and the NBS instability was reduced by the decrease of the electron density in the IGZO layer owing to the ejection of H donor-like defects from IGZO.

Acknowledgments: This research was supported by the Academic Research Fund of Hoseo University in 2016 (20160043).

References and Notes

1. K. Nomura, H. Ohta, K. Ueda, T. Kamiya, M. Hirano, and H. Hosono, *Science* 300, 1269 (**2003**).
2. K. Nomura, T. Kamiya, H. Ohta, T. Uruga, M. Hirano, and H. Hosono, *Phys. Rev. B* 75, 35212 (**2007**).
3. K. Abe, N. Kaji, H. Kumomi, K. Nomura, T. Kamiya, M. Hirano, and H. Hosono, *IEEE Trans. Electron. Devices* 58, 3463 (**2011**).
4. J. Jeong, J. Kim, G. J. Lee, and B.-D. Choi, *Appl. Phys. Lett.* 100, 023506 (**2012**).
5. M. Mativenga, S. An, S. Lee, J. Um, D. Geng, R. K. Mruthyunjaya, G. N. Heiler, and T. J. Tredwell, *IEEE Trans. Electron. Devices* 61, 2106 (**2014**).
6. E. T. Kim, C.-K. Kim, M. K. Lee, T. W. Bang, Y.-K. Choi, S.-H. Ko Park, and K. C. Choi, *Appl. Phys. Lett.* 108, 182104 (**2016**).
7. L. Petti, N. Münzenrieder, C. Vogt, H. Faber, L. Büthe, G. Cantarella, F. Bottacchi, T. D. Anthopoulos, and G. Tröster, *Appl. Phys. Rev.* 3, 021303 (**2016**).
8. X. Ding, F. Huang, S. Li, J. Zhang, X. Jiang, and Z. Zhang, *Electron. Mater. Lett.* 13, 45 (**2017**).
9. H. Oh, S.-H. Ko Park, C.-S. Hwang, S. Yang, and M. K. Ryu, *Appl. Phys. Lett.* 99, 022105 (**2011**).
10. W.-T. Chen, S.-Y. Lo, S.-C. Kao, H.-W. Zan, C.-C. Tsai, J.-H. Lin, C.-H. Fang, and C.-C. Lee, *IEEE Eectron. Dev. Lett.* 32, 1552 (**2011**).
11. R. Zhan, C. Dong, P.-T. Liu, and H.-P. D. Shieh, *Microelectronics Reliability* 53, 1879 (**2013**).
12. J. P. Bermundo, Y. Ishikawa, H. Yamazaki, T. Nonaka, and Y. Uraoka, *ECS J. Solid State Sci. and Technol.* 3, Q16 (**2014**).
13. J. P. Bermundo, Y. Ishikawa, H. Yamazaki, T. Nonaka, M. N. Fujii, and Y. Uraoka, *Appl. Phys. Lett.* 107, 33504 (**2015**).
14. S. H. Cho, M. J. Choi, K. B. Chung, and J. S. Park, *Electron. Mater. Lett.* 11, 360 (**2015**).
15. T. Oh, *Electron. Mater. Lett.* 11, 853 (**2015**).
16. R. Zhan, C. Dong, P.-T. Liu, and H.-P. D. Shieh, *Microelectronics Reliability* 53, 1879 (**2013**).
17. J. P. Bermundo, Y. Ishikawa, H. Yamazaki, T. Nonaka, and Y. Uraoka, *ECS J. Solid State Sci. Technol.* 3, Q16 (**2014**).
18. J. P. Bermundo, Y. Ishikawa, H. Yamazaki, T. Nonaka, M. N. Fujii, and Y. Uraoka, *Appl. Phys. Lett.* 107, 33504 (**2015**).
19. J. Wu, Y. Chen, D. Zhou, Z. Hu, H. Xie, and C. Dong, *Mater. Sci. Semicond. Process.* 29, 277 (**2015**).
20. J. Li, F. Zhou, H.-P. Lin, W.-Q. Zhu, J.-H. Zhang, X.-Y. Jiang, and Z.-L. Zhang, *Vaccum* 86, 1840 (**2012**).
21. S.-Y. Huang, T.-C. Chang, M.-C. Chen, T.-C. Chen, F.-Y. Jian, Y.-C. Chen, H.-C. Huang, and D.-S. Gan, *Surface and Coatings Technology* 231, 117 (**2013**).
22. D. Y. Yoo, E. Chong, D. H. Kim, B. K. Ju, and S. Y. Lee, *Thin Solid Films* 520, 3783 (**2012**).
23. Z. Hu, D. Zhou, L. Xu, Q. Wu, H. Xie, and C. Dong, *Solid-State Electronics* 104, 39 (**2015**).
24. J. K. Jeong, H. W. Yang, J. H. Jeong, Y. G. Mo, and H. D. Kim, *Appl. Phys. Lett.* 93, 123508 (**2008**).
25. G.-W. Chang, T.-C. Chang, Y.-E. Syu, T.-M. Tsai, K.-C. Chang, C.-H. Tu, F.-Y. Jian, Y.-C. Hung, and Y.-H. Tai, *Thin Solid Films* 520, 1608 (**2011**).
26. S.-H. Choi, J.-H. Jang, K. Jang-Joo, and M.-K. Han, *IEEE Electron. Device Lett.* 33, 381 (**2012**).
27. http://www.nepes.co.kr/web/nepes_eng/em2.
28. J. J. Dong, X. W. Zhang, J. B. You, P. F. Cai, Z. G. Yin, Q. An, X. B. Ma, P. Jin, Z. G. Wang, and P. K. Chu, *ACS Appl. Mater. Interf.* 2, 1780 (**2010**).
29. T. Toda, D. Wang, J. Jiang, M. P. Hung, and M. Furuta, *IEEE Trans. Electron. Devices* 61, 3762 (**2014**).

Received: 27 October 2016. Accepted: 9 March 2017.